Atmospheric
Chemistry
and Physics
Discussions

Open Access

1 Chemical characteristics and causes of airborne particulate pollution

2 in warm seasons in Wuhan, central China

3

4 X.P. Lyu[1], N. Chen[2], H. Guo[1*], L.W. Zeng[1], W.H. Zhang[3], F. Shen[2], J.H. Quan[2], N. Wang[4]

5 [1] Department of Civil and Environmental Engineering, The Hong Kong Polytechnic

6 University, Hong Kong

7 [2] Hubei Provincial Environment Monitoring Center, Wuhan, China

8 3 Department of Environmental Sciences, School of Resource and Environmental Sciences,

9 Wuhan University, Wuhan, China

10 4 Guangdong Provincial Key Laboratory of Regional Numerical Weather Prediction, Institute

11 of Tropical and Marine Meteorology, Guangzhou, China

12 *Corresponding author. Tel: +852 3400 3962; Fax: +852 2334 6389; Email:

13 ceguohai@polyu.edu.hk

14

15 **Abstract:** Continuous measurements of airborne particles and their chemical compositions

16 were conducted in May, June, October and November 2014 at an urban site in Wuhan,

17 Central China. The results indicated that the particle concentrations stayed at a relatively high

18 level in Wuhan, with the averages of 135.1 ± 4.4 (mean±95% interval) and 118.9 ± 3.7 μg/m^3

19 for PM_{10}, and 81.2 ± 2.6 and 85.3 ± 2.6 μg/m^3 for $PM_{2.5}$ in summer and autumn, respectively.

20 Moreover, $PM_{2.5}$ frequently exceeded the National Standard Level II (*i.e.,* daily average of 75

21 μg/m^3), and six $PM_{2.5}$ episodes were captured during the sampling campaign. The

22 composition analysis found that secondary inorganic ions and carbonaceous aerosols

23 dominated the constituents of $PM_{2.5}$. It is noteworthy that potassium (K) $(2060.7 \pm 82.3$

24 ng/m^3, $47.0 \pm 2.2\%$) was the most abundant element, implying the biomass burning in/around

25 Wuhan. During the episodes, carbonaceous aerosols increased significantly, a signature of

26 combustion activities as well. The source apportionment confirmed that biomass burning was

27 the main cause of $PM_{2.5}$ episodes except for case 2, with the contribution ranging from $48.0 \pm$

28 1.0% in case 5 to $70.1 \pm 0.5\%$ in case 3. Fugitive dust and oil refinery/usage were the main

29 contributors to $PM_{2.5}$ in case 2. In addition to biomass burning, the contribution of oil

Atmospheric
Chemistry
and Physics
Discussions

Open Access

EGU

30 refinery/usage also increased in case 5. Furthermore, the mass and proportion of NO_3^- peaked

31 in case 6. It was found that the high levels of NO_x and NH_3, and low temperature in case 6

32 were responsible for the increment of NO_3^-. We also found that SOC formation was

33 dominated by the aromatics and isoprene in autumn, and the contribution of aromatics

34 increased during the episodes.

35 **Keywords:** $PM_{2.5}$; NO_3^-; SOA; biomass burning; formation mechanism

36

37 **1. Introduction**

38 Airborne particulate pollution is distinguished by high levels of particle concentrations in the

39 atmosphere. With typical characteristics of reducing visibility and building up of particle

40 concentrations, airborne particulate pollution is also called "haze", which swept across the

41 whole China in recent years, particularly the northern, central and eastern China (Cheng et al.,

42 2014; Kang et al., 2013; Wang et al., 2013). Due to its detrimental effects on human health

43 (Anderson et al., 2012; Goldberg et al., 2001), atmospheric environment (Yang et al., 2012;

44 White and Roberts, 1977), acid precipitation (Zhang et al., 2007; Kerminen et al., 2001) and

45 climate change (Ramanathan etal., 2001; Nemesure et al., 1995), particulate pollution has

46 become major concerns of scientific communities and local governments. The China's

47 National ambient air quality standards issued in 2012 regulate the annual upper limit of PM_{10}

48 (*i.e.*, particulate matter with aerodynamic diameter less than 10 μm) and $PM_{2.5}$ (*i.e.*,

49 particulate matter with aerodynamic diameter less than 2.5 μm) as 70 and 35 μg/m^3, and 24-h

50 average as 150 and 75 μg/m^3, respectively (GB 3095-2012).

51 Numerous studies focused on the spatial and temporal variations of particle concentrations,

52 the chemical compositions and the cause analysis of haze events (Cheng et al., 2014; Cao et

53 al., 2012; Zheng et al., 2005; Yao et al., 2002). Generally, the particulate pollution was

54 severer in winter due to the additional emissions (*e.g.* coal burning) and unfavorable

55 dispersion conditions (Lyu et al., 2015a; Zheng et al., 2005). And northern China often

56 suffers heavier, longer and more frequent haze pollution than southern China (Cao et al.,

57 2012). The chemical analysis indicated that secondary inorganic aerosol (SIOA), *i.e.*, sulfate

58 (SO_4^{2-}), nitrate (NO_3^-) and ammonia (NH_4^+), and secondary organic aerosol (SOA) dominated

59 the total mass of airborne particles (Zhang et al., 2014; Zhang et al., 2012). However, the

Atmospheric
Chemistry
and Physics
Discussions

60 composition differed among the size-segregated particles. In general, the secondary

61 components were prone to be accumulated in small particles, in contrast to the phenomenon

62 that crustal elements were more enriched in larger particles (Zhang et al., 2013; Theodosi et

63 al., 2011). Indeed, the general characteristics of particles (*i.e.*, toxicity, radiative forcing,

64 acidity, etc.) are all tightly associated with the chemical compositions and physical sizes,

65 which therefore have been extensively studied in the field of aerosols. To better understand

66 and control airborne particulate pollution, the causes and formation mechanisms were often

67 investigated (Wang et al., 2014a and b; Kang et al., 2013; Oanh and Leelasakultum, 2011).

68 Apart from the unfavorable meteorological conditions, emission enhancement was often the

69 major culprit. With no doubt, industrial and vehicular emissions contributed greatly to the

70 particle mass through direct emission and secondary formation of particles from gaseous

71 precursors, such as sulfur dioxide (SO_2), nitrogen oxides (NO_x) and volatile organic

72 compounds (VOCs) (Guo et al., 2011a). In addition, some other sources in specific regions or

73 during specific time periods also remarkably built up the particle concentrations, *e.g.* coal

74 combustion in north China (Cao et al., 2005; Zheng et al., 2005) and biomass burning in

75 Southeast Asia (Deng et al., 2008; Koe et al., 2001). Furthermore, some studies explored the

76 possible formation mechanisms of main particle components, *i.e.,* SIOA and SOA, and

77 distinguished the contributions of different formation pathways. For example, Wang et al.

78 (2014) demonstrated that heterogeneous oxidation of SO_2 on aerosol surfaces was an

79 important supplementary pathway to particle-bound SO_4^{2-} in addition to the gas phase

80 oxidation and reactions in cloud. On the other hand, it was reported that homogeneous and

81 heterogeneous reactions dominated the formation of NO_3^- in daytime and nighttime,

82 respectively (Pathak et al., 2011; Lin et al., 2007; Seinfeld and Pandis, 1998). Furthermore,

83 biogenic VOCs and aromatics were proved to be the main precursors of SOA (Kanakidou et

84 al., 2005; Forstner et al., 1997).

85 Despite numerous studies, the full components of airborne particles were seldom reported

86 due to the cost of sampling and chemical analysis, resulting in a gap for comprehensive

87 understanding of chemical characteristics of particles. Additionally, although the causes of

88 particle episodes were often discussed in many case studies (Wang et al., 2014; Deng et al.,

89 2008), the contribution was rarely quantified. Furthermore, the formation mechanisms might

Atmospheric
Chemistry
and Physics
Discussions

90   be distinctive in different circumstances. Therefore, an overall understanding of chemical

91   characteristics of airborne particles, the cause analysis of the particle episodes and formation

92   mechanisms of the enhanced species are of great value. In addition, it has become a regular

93   phenomenon in central China that haze pollution occurred frequently in warm seasons, while

94   the causes were not identified and the contributions were not quantified. Wuhan is the largest

95   megacity in central China, and has been suffering from severe particulate pollution in recent

96   years. Data indicated that the frequency of $PM_{2.5}$ exceeding the national standard level II (*i.e.*,

97   daily average of 75 $\mu g/m^3$) in Wuhan reached 55.1% in 2014 (Wuhan Environmental Bulletin,

98   2014). In warm seasons of 2014, the hourly maximum $PM_{2.5}$ (564 $\mu g/m^3$) was even higher

99   than that in winter (383 $\mu g/m^3$), as shown in Figure S1 in the supplementary material.

100   Moreover, as the air quality in Wuhan is strongly influenced by the surrounding cities, the

101   pollution level in Wuhan also reflects the status of the city clusters in central China. However,

102   previous studies (Lyu et al., 2015a; Cheng et al., 2014) were insufficient to fully understand

103   the properties of airborne particles in this region, particularly in warm seasons, not to mention

104   guiding the control strategies. As such, it is urgent to grasp the chemical characteristics of

105   airborne particles, and to explore the causes and formation mechanisms of the particle

106   episodes in Wuhan.

107   This study deeply analyzed the chemical characteristics of $PM_{2.5}$ in Wuhan from a full suite

108   of component measurement data, *i.e.*, SO_4^{2-}, NO_3^-, NH_4^+, organic carbon (OC) including

109   primary organic carbon (POC) and secondary organic carbon (SOC), element carbon (EC)

110   and metal elements. Furthermore, based on the analysis of meteorological conditions,

111   chemical signatures, source apportionment and fire spot distribution, the causes of the $PM_{2.5}$

112   episodes were identified and the contributions were quantified. Lastly, this study utilized a

113   photochemical box model incorporating master chemical mechanism (PBM-MCM) and

114   theoretical calculation to investigate the formation processes of NO_3^- and SOC. It is the first

115   study to quantify the contribution of biomass burning to $PM_{2.5}$, and probe into the formation

116   mechanisms of both inorganic and organic components in $PM_{2.5}$ in central China.

117

118   **2. Methodology**

119   **2.1 Data collection**

Atmospheric
Chemistry
and Physics
Discussions

120   The whole set of air pollutants were continuously monitored at an urban site in the largest

121   megacity of central China, *i.e.*, Wuhan. The measurement covered two periods, *i.e.*, May-June

122   in summer and October-November in autumn of 2014. The measured species included

123   particle-phase pollutants such as PM_{10}, $PM_{2.5}$ and particle-bound components and gas-phase

124   pollutants, *i.e.*, VOCs, SO_2, CO, NO, NO_2, O_3, HNO_3 (g), NH_3 (g), HCl (g) and etc. The

125   sampling site (30.54N, 114.37E) was set up in the Hubei Environmental Monitoring Center

126   Station, as shown in Figure 1, located in a mixed commercial and residential area, where

127   industries were seldom permitted. The instruments were housed in a room of a six-story

128   building (~18 m a.g.l.), adjacent to a main road with the straight-line distance of

129   approximately 15 m.

130   PM_{10} and $PM_{2.5}$ were measured by a continuous ambient particulate monitor (Thermo

131   Fisher-1405D, USA). The water soluble ions (WSIs) in $PM_{2.5}$ and gases including HNO_3,

132   HCl and NH_3 were detected using the online ion chromatography monitor

133   (Metrohm-MARGA 1S, Switzerland), and an aerosol OC/EC online analyzer (Sunset-RT-4,

134   USA) using the thermal/optical analysis technique was utilized to resolve the carbonaceous

135   aerosols (OC and EC). In addition, the elements in $PM_{2.5}$ were measured with a customized

136   metal analyzer, which combined the X-ray fluorescence and beta-ray absorption detection

137   techniques. For the analysis of trace gases, *i.e.*, SO_2, CO, NO, NO_2 and O_3, a suite of

138   commercial analyzers developed by Thermo Environmental Instruments (TEI) Inc. were used,

139   which have been described in details in previous studies (Lyu et al. 2016; Geng et al., 2009).

140   Furthermore, a gas chromatography-flame ionization detector-mass spectrometry

141   (GC-FID-MS) system (TH_PKU-300) was used to resolve the real time data of ambient

142   VOCs. Details about the analysis techniques, resolution, detection limits and the protocol of

143   quality assurance/control have been provided in Lyu et al. (2016) and Wang et al. (2014).

Atmospheric
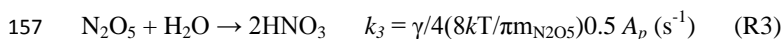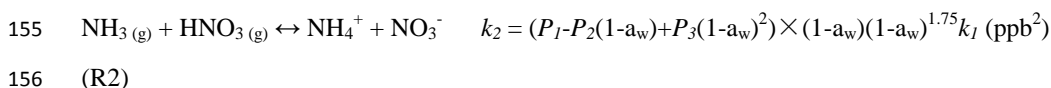Chemistry
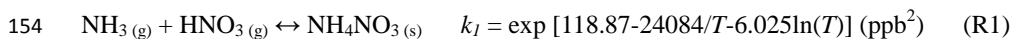and Physics
Discussions

Open Access
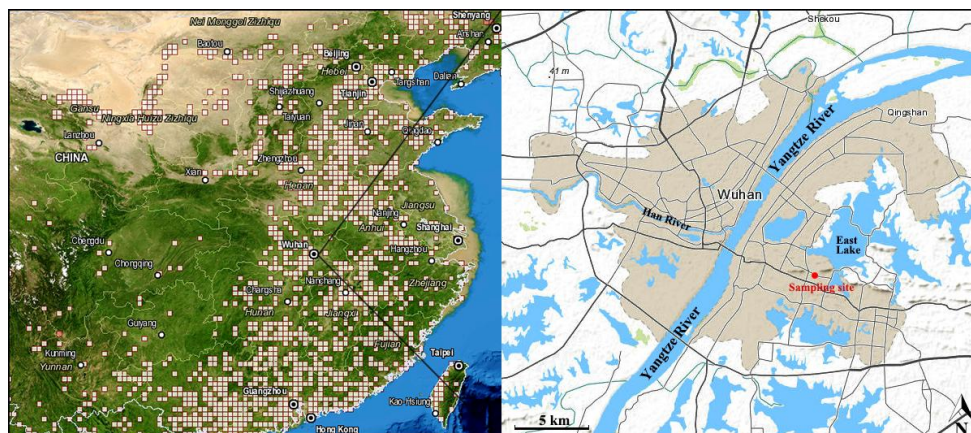
144

145   Figure 1 Geographic location of the sampling site. The white blocks in the left panel represent the

146   total distribution of fire spots in autumn 2014 in China, and the urban area in Wuhan is highlighted

147   with grey color in the right panel.

148   **2.2 Theoretical calculation and model simulation**

149   Theoretical calculation and model simulation were applied in this study to probe into the

150   formation mechanisms of NO_3^- and SOC. The particle-bound NO_3^- was generally combined

151   with NH_3 or presented as HNO_3 in the ammonia deficit environment, following the processes

152   described in R1-R3 after HNO_3 was formed through the oxidation of NO_x (Pathak et al., 2011,

153   Lin et al., 2010). The production of NO_3^- can be calculated by Equations 1-4.

154    $NH_{3\,(g)} + HNO_{3\,(g)} \leftrightarrow NH_4NO_{3\,(s)}$ $k_1 = \exp[118.87-24084/T-6.025\ln(T)]$ (ppb^2)   (R1)

155    $NH_{3\,(g)} + HNO_{3\,(g)} \leftrightarrow NH_4^+ + NO_3^-$ $k_2 = (P_1-P_2(1-a_w)+P_3(1-a_w)^2)\times(1-a_w)(1-a_w)^{1.75}k_1$ (ppb^2)

156   (R2)

157    $N_2O_5 + H_2O \rightarrow 2HNO_3$ $k_3 = \gamma/4(8kT/\pi m_{N2O5})0.5\,A_p$ (s^{-1})   (R3)

158    $\ln(P_1) = -135.94 + 8763/T + 19.12\ln(T)$ (Eq.1)

159    $\ln(P_2) = -122.65 + 9969/T + 16.22\ln(T)$ (Eq.2)

160    $\ln(P_3) = -182.61 + 13875/T + 24.46\ln(T)$ (Eq.3)

161    $[NO_3^-] = 0.775\left(\dfrac{[NH_3]+[HNO_3]-\sqrt{([NH_3]+[HNO_3])^2-4([NH_3][HNO_3]-k_1(k_2))}}{2}\right)$ (Eq.4)

162   where R1 and R2 describe the homogeneous formation of NO_3^- under the humidity of lower

163   and higher than deliquescence relative humidity (DRH) of NH_4NO_3 (*i.e.*, 62% (Tang and

164   Munkelwitz, 1993)), respectively. R3 presents the heterogeneous reaction of N_2O_5 on the

165   pre-existing aerosol surfaces. k_{1-3} represent the rate of reactions R*1-3*. *T*, a_w and *P* are the

Atmospheric
Chemistry
and Physics
Discussions

Open Access

166 temperature, relative humidity and the temperature-related coefficient, respectively. In R3, γ

167 is the reaction probability of N_2O_5 on aerosol surfaces, assigned as 0.05 and 0.035 on the

168 surface of sulfate ammonia and element carbon, respectively (Aumont et al., 1999; Hu and

169 Abbatt, 1997). k is the Boltzmann constant (1.38×10^{-23}), m_{N2O5} is the molecular mass of

170 N_2O_5 (1.79×10^{-22} g), and A_p is the aerosol specific surface area (cm^2/cm^3).

171 Furthermore, the PBM-MCM model was used to simulate the oxidation products in this study,

172 namely O_3, N_2O_5 and semi- VOCs (SVOCs), and radicals like OH, HO_2 and RO_2. With full

173 consideration of photochemical mechanisms and real meteorological conditions, the model

174 has been successfully applied in the study of photochemistry. Details about the model

175 construction and application can be found in Lyu et al. (2015b), Ling et al. (2014) and Lam et

176 al. (2013).

177 **2.3 Source apportionment model**

178 The positive matrix factorization (PMF) model was utilized to resolve the sources of $PM_{2.5}$.

179 As a receptor model, PMF has been extensively used in the source apportionment of airborne

180 particles and VOCs (Brown et al., 2007; Lee et al., 1999). Detailed introductions about the

181 model can be found in Paatero (1997) and Paatero and Tapper (1994). Briefly, it decomposes

182 the input matrix (X) into the matrices of factor contribution (G) and factor profile (F) in p

183 sources, as shown in Equation 5. A statistic value (Q) (Equation 6) was aromatically

184 generated to guide the selection of the best run when the lowest Q was obtained.

185 $x_{ij} = \sum_{k=1}^{p} g_{ik} f_{kj} + e_{ij}$ (Eq.5)

186 $Q = \sum_{i=1}^{n} \sum_{j=1}^{m} \left[\dfrac{x_{ij} - \sum_{k=1}^{p} g_{ik} f_{kj}}{u_{ij}} \right]^2$ (Eq.6)

187 where x_{ij} and u_{ij} are the concentration and uncertainty of j species (total of m) in i sample

188 (total of n), g_{ik} represents the contribution of k_{th} source to i sample, f_{kj} indicates the

189 fraction of j species in k_{th} source, and e_{ij} is the residual for j species in i sample.

190

191 **3. Results and discussion**

192 **3.1 Concentrations of PM_{10} and $PM_{2.5}$**

193 Table 1 shows the mean concentrations of PM_{10} and $PM_{2.5}$ in Wuhan and other Chinese cities/

194 regions. The average, maximum and minimum values, standard deviation or 95% confidence

195   interval (C.I.) were provided if available. Generally, the concentrations of airborne particles

196   in Wuhan (135.1 ± 4.4 and 118.9 ± 3.7 $\mu g/m^3$ for PM_{10}; 81.2 ± 2.6 and 85.3 ± 2.6 $\mu g/m^3$ for $PM_{2.5}$

197   in summer and autumn, respectively) were lower than those in northern China (*i.e.*, Beijing

198   and Xi'an), comparable to those in eastern China (*i.e.*, Shanghai and Nanjing), and higher

199   than those in southern China (*i.e.*, Guangzhou and Hong Kong) and Taiwan. Indeed, the

200   sampling site, period, method and instrument all interfered with the inter-comparisons.

201   Bearing these factors in mind, the ambient particulate pollution in Wuhan was severe.

202   From summer to autumn, PM_{10} experienced a considerable reduction from 135.1 ± 4.4 to

203   118.9 ± 3.7 $\mu g/m^3$, while $PM_{2.5}$ remained statistically stable. This suggested that the emission

204   strength of coarse particles weakened in autumn as compared to that in summer, perhaps

205   related to the variations of the number of construction sites. Fugitive dust was a common

206   source of coarse particles, confirmed in previous studies conducted in Wuhan (Lyu et al.,

207   2015a; Cheng et al., 2014). Meteorological conditions were another factor for the reduction.

208   However, there was no significant difference in relative humidity between summer ($59.7 \pm$

209   0.7%) and autumn ($60.4 \pm 0.8\%$) ($p > 0.05$), and the frequency of rainy days in summer

210   (50.8%) was even higher than that in autumn (36.1%). Therefore, the lower PM_{10} level in

211   autumn might benefit from the lower wind speed (1.2 ± 0.04 and 0.8 ± 0.03 m/s in summer

212   and autumn, respectively; $p < 0.05$) and temperature (25.6 ± 0.2 and 17.5 ± 0.3 ℃ in summer

213   and autumn, respectively; $p < 0.05$).

214   Table 1 Comparisons of PM_{10} and $PM_{2.5}$ between Wuhan and other Chinese cities/ regions (Unit:

215    $\mu g/m^3$)

	PM_{10}	$PM_{2.5}$	Sampling period
Wuhan	135.1 ± 4.4	81.2 ± 2.6	May-Jun. 2014 (this study)
	118.9 ± 3.7	85.3 ± 2.6	Oct.-Nov. 2014 (this study)
Beijing	155.9	73.8	Jun.-Aug. 2009 [a]
	194.4	103.9	Sept.-Nov. 2009 [a]
	133.7 ± 87.8	71.5 ± 53.6	2012 whole year [b]
Xi'an	257.8 ± 194.7	140.9 ± 108.9	2011 whole year [c]
Shanghai	97.4-149.2	62.3-103.1	Jul. 2009-Sept. 2010 [d]

Atmospheric
Chemistry
and Physics
Discussions

Nanjing	119-171	87-125	Jun. 2012 [e]
Guangzhou	23.4	19.2	Jun.-Aug. 2010-2013 [f]
	51.0	41.3	Sept.-Nov. 2010-2013 [f]
Hong Kong	31.0 ± 16.7	17.7 ± 12.9	Jun.-Aug. 2014 [g]
	55.8 ± 23.6	34.0 ± 17.3	Sept.-Nov. 2014 [g]
Tai Wan	39.5 ± 11.6	21.8 ± 7.5	May-Nov. 2011 [h]

216   [a] Liu et al. (2014); [b] Liu et al. (2015); [c] Wang et al. (2015); [d] Wang et al. (2013); [e] Shen et al.

217   (2014); [f] Deng et al. (2015); [g] HKEPD (2014); [h] Gugamsetty et al. (2012).

218

219   Figure 2 presents the daily concentrations of PM_{10} and $PM_{2.5}$ during the sampling period in

220   Wuhan, with the National Standard Level II (daily averages of 150 and 75 $\mu g/m^3$ for PM_{10}

221   and $PM_{2.5}$, respectively). It was found that the concentrations of PM_{10} and $PM_{2.5}$ frequently

222   exceeded the standard levels, indicating the significance of ambient particulate pollution in

223   Wuhan. Due to the fact that the chemical, optical and toxic properties tend to be more

224   apparent in smaller particles (Yang et al., 2012; Goldberg et al., 2001), and the $PM_{2.5}$

225   components were completely resolved, this work mainly focused on the study of $PM_{2.5}$.

226   During the sampling campaign, six $PM_{2.5}$ episodes named as case 1 – case 6 with the daily

227   averages of $PM_{2.5}$ exceeding 75 $\mu g/m^3$ were captured (Figure 2). It should be noted that to

228   ensure the data size of each episode, only the cases in which the daily $PM_{2.5}$ was

229   consecutively higher than 75 $\mu g/m^3$ for ≥3 days were treated as $PM_{2.5}$ episodes.

230   Table 2 summarizes the concentrations of PM_{10} and $PM_{2.5}$, and the percentage of $PM_{2.5}$ in

231   PM_{10}, referred to $PM_{2.5}/PM_{10}$, during the summer and autumn episodes and non-episodes. It

232   was found that PM_{10} and $PM_{2.5}$ increased significantly ($p<0.05$) during the episodes in both

233   summer and autumn. $PM_{2.5}/PM_{10}$ was a measure of the proportion of secondary species in

234   particles. Generally, higher $PM_{2.5}/PM_{10}$ indicates higher content of secondary aerosols, which

235   tend to be accumulated in smaller particles. Compared to those during non-episodes (58.9 ±

236   1.5% and 65.3 ± 1.3% in summer and autumn, respectively), $PM_{2.5}/PM_{10}$ increased

237   remarkably on episode days except for case 2 (45.9 ± 2.5%), indicating that secondary

238   species were more enhanced during the episodes. However, the lowest $PM_{2.5}/PM_{10}$ in case 2

Atmospheric
Chemistry
and Physics
Discussions

239   might imply a strong source of coarse particles. Indeed, significant contribution of fugitive

240   dust (5.0 ± 0.3 μg/m^3; $17.6 \pm 1.2\%$) was identified in case 2 (see details in section 3.3.3).

241
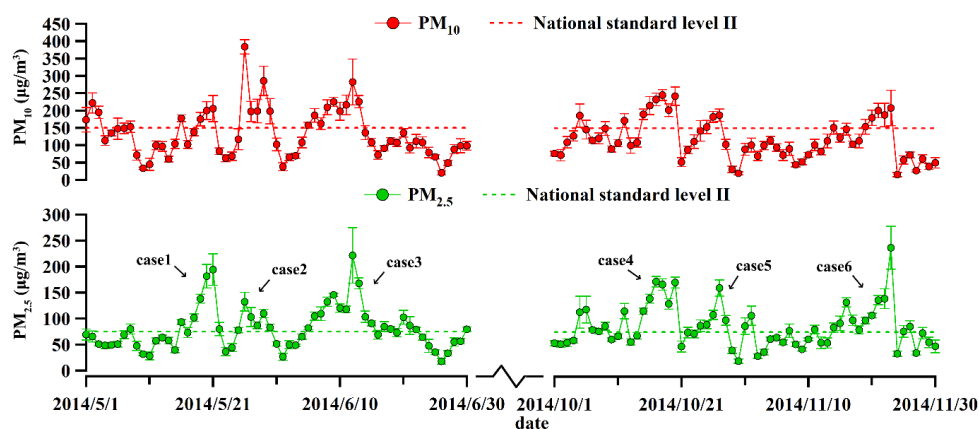
243   Figure 2 Daily concentrations of PM$_{10}$ and PM$_{2.5}$ in May, June, October and November 2014. Case 1:

244   May 16-22, case 2: May 25-30; case 3: June 5-15; case 4: October 15-20; case 5: October 24-28; Case

245   6: November 14-23.

246

247   Table 2 PM$_{10}$, PM$_{2.5}$ and PM$_{2.5}$/PM$_{10}$ with 95% C.I. during PM$_{2.5}$ episodes and non-episodes in Wuhan.

248   Non-episode 1 and Non-episode 2 represent the non-episode period in summer and autumn,

249   respectively.

|	PM$_{10}$ (μg/m^3)	PM$_{2.5}$ (μg/m^3)	PM$_{2.5}$/PM$_{10}$ (%)
Case 1	154.3 ± 10.1	123.0 ± 9.1	72.8 ± 2.6
Case 2	230.1 ± 19.1	98.9 ± 5.7	45.9 ± 2.5
Case 3	191.4 ± 9.8	126.7 ± 7.0	66.9 ± 1.8
Non-episode 1	**98.5 ± 3.9**	**56.6 ± 1.7**	**58.9 ± 1.5**
Case 4	221.8 ± 8.9	148.6 ± 5.2	67.9 ± 2.0
Case 5	154.2 ± 10.4	108.2 ± 6.8	69.3 ± 3.1
Case 6	157.3 ± 9.0	120.0 ± 7.6	71.2 ± 2.1
Non-episode 2	**88.7 ± 3.4**	**64.2 ± 2.2**	**65.3 ± 1.3**

250

251   **3.2 Chemical composition of PM$_{2.5}$**

3.2.1 Overall characteristics

252

253 Figure 3 shows the daily variations of $PM_{2.5}$ and its composition. Since the instrument for the

254 analysis of WSIs was initially deployed in September 2014, the data was not available in May

255 and June. The carbonaceous aerosol (18.5 ± 1.2 μg/m^3) and elements (6.0 ± 0.3 μg/m^3)

256 accounted for 19.1 ±0.6% and 6.2 ±0.2% of $PM_{2.5}$ in summer, respectively. In autumn, WSIs

257 was the most abundant component in $PM_{2.5}$ (64.4 ± 2.5 μg/m^3; 68.6 ± 1.9%), followed by

258 carbonaceous aerosol (24.3 ± 1.0 μg/m^3; 25.5 ± 0.8%) and elements (4.5 ± 0.2 μg/m^3; 4.6 ±

259 0.1%). Secondary inorganic ions SO_4^{2-} (18.8 ± 0.6 μg/m^3), NO_3^- (18.7 ± 0.8 μg/m^3) and NH_4^+

260 (12.0 ± 0.4 μg/m^3) dominated in WSIs, with the average contribution of 34.0 ±0.6%, 30.1 ±

261 0.5% and 20.4 ± 0.1%, respectively. Generally, the relative abundance of SO_4^{2-} and NO_3^-

262 reflected the contribution of stationary and mobile sources to $PM_{2.5}$ (Arimoto et al., 1996).

263 The comparable levels of SO_4^{2-} and NO_3^- indicated that stationary source and mobile source

264 made equivalent contribution to $PM_{2.5}$ in Wuhan.
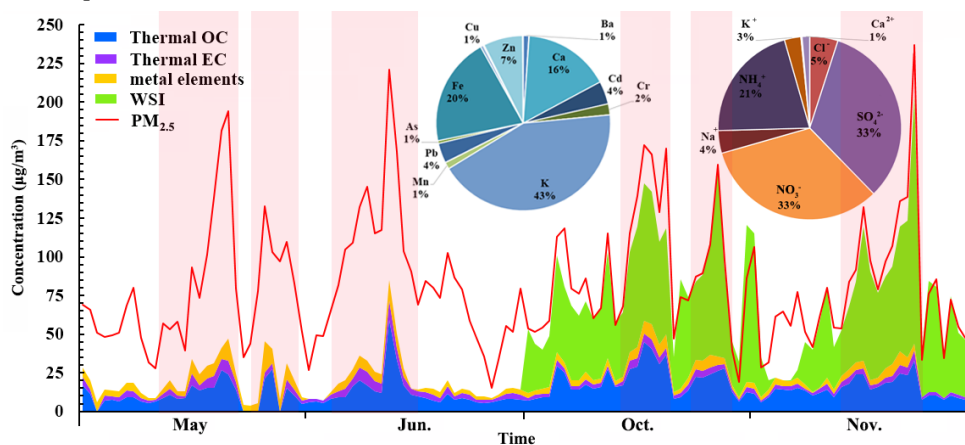
265

266 Figure 3 Daily variations of $PM_{2.5}$ and its components. The inserted pie charts represent the

267 composition of elements and water soluble ions, respectively. The red highlighted areas represent the

268 episodes.

269 The charge balance between the anions and cations was usually used to predict the existing

270 forms of the secondary inorganic ions in $PM_{2.5}$. Figure 4 shows the relative abundance of

271 molar charges of the anions (*i.e.*, SO_4^{2-} and NO_3^-) and the cation (*i.e.*, NH_4^+). The data were

272 located fairly close to the one-to-one line, regardless of episode or non-episode days. This

273 suggested that NH_4NO_3 and $(NH_4)_2SO_4$ were the co-existing forms of the secondary

Atmospheric
Chemistry
and Physics
Discussions

274   inorganic ions in $PM_{2.5}$ in Wuhan.
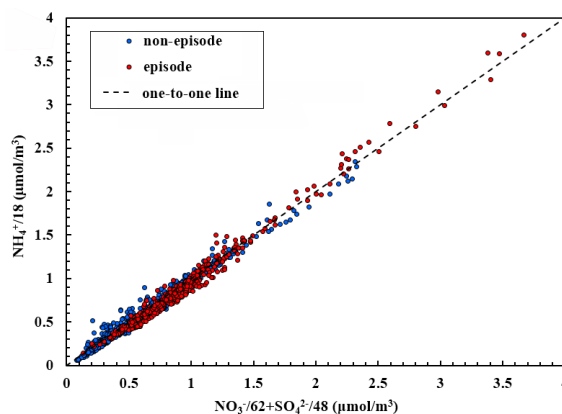
275

276   Figure 4 Charge balance between of the secondary inorganic ions in $PM_{2.5}$

277

278   For the carbonaceous aerosol, OC (14.8 ± 0.5 $\mu g/m^3$) and EC (3.6 ± 0.1 $\mu g/m^3$) accounted for

279    $79.9 \pm 0.3\%$ and $20.2 \pm 0.3\%$ of the total carbon, respectively. Generally, SOC was expected

280   to exist when OC/EC was larger than 2, and the proportion of SOC increased with the

281   increase of OC/EC ratios (Duan et al., 2005; Chow et al., 1996). The average OC/EC ratio

282   was 4.8 ± 0.1 in Wuhan, suggesting that SOC (*i.e.*, carbon fraction of SOA) was an important

283   component in $PM_{2.5}$. Indeed, as the constituents of OC, SOC and POC can be distinguished

284   with the EC-tracer method, following Equations 7 and 8 (Cabada et al., 2004):

285    $POC = (OC/EC)_{prim} \times EC + OC_{non-comb}$ (Eq.7)

286    $SOC = OC - POC$ (Eq.8)

287   where $(OC/EC)_{prim}$ was obtained from certain pairs of OC and EC with the OC/EC ratios

288   among the 10% lowest, and $OC_{non-comb}$ represented the non-combustion related OC. Figure 5

289   shows the linear regressions between the eligible OC and EC, where the slope and the

290   intercept indicated the $(OC/EC)_{prim}$ and $OC_{non-comb}$, respectively. Since the abundance of

291   SOC depended largely upon the oxidative capacity of the atmosphere, the oxidative radical

292   (HO_2) was simulated by the PBM-MCM model and compared with the pattern of SOC. More

293   details about the simulation were provided in section 3.4. Figure 6 shows the hourly

294   concentrations of SOC and POC, and the average diurnal patterns of SOC, POC and HO_2. In

295   general, POC (8.6 ± 0.2 $\mu g/m^3$) was slightly higher than SOC (6.4 ± 0.3 $\mu g/m^3$) (*p* value?).

Atmospheric
Chemistry
and Physics
Discussions

296   The difference reached the highest in November when the concentration was 9.5 ± 0.4 and

297   4.7 ± 0.3 µg/m^3 for POC and SOC, respectively. Since the production of SOC was closely

298   related to the atmospheric oxidative capacity, the lowest fraction of SOC in November might

299   be attributable to the weakest oxidative capacity, *e.g.*, O_3 was the lowest in November ($14.3 \pm$

300   1.0 ppbv). The diurnal patterns of POC and SOC revealed that POC was relatively stable

301   throughout the day. The increase of POC in the early morning (06:00-08:00) and late

302   afternoon (16:00-20:00) was likely related to the enhanced vehicular emissions in the rush

303   hours, and the decrease from 08:00-15:00 might be caused by the extension of the boundary

304   layer. In contrast, SOC showed two peaks at ~12:00 and 19:00, which was consistent with the

305   diurnal variation of the simulated HO_2, suggesting that the formation of SOC was closely

306   related to the oxidative radicals in the atmosphere (detailed relationship was discussed in

307   section 3.4.3).
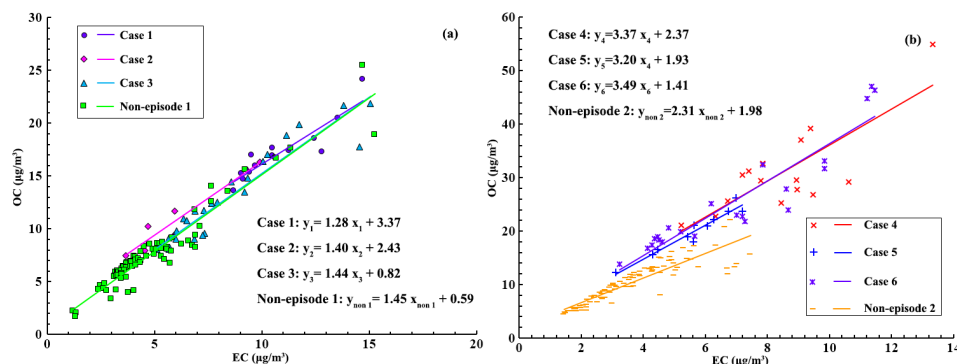
308

309   Figure 5 Regression between OC and EC with the 10% lowest OC/EC ratios in (a) summer and (b)

310   autumn in Wuhan

311

13

Atmospheric
Chemistry
and Physics
Discussions
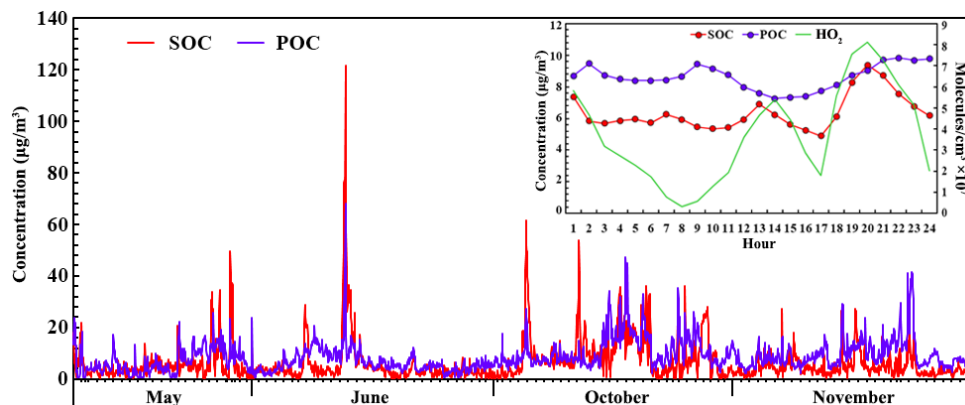
312   Figure 6 Hourly concentrations of SOC and POC. The insert graph presents the average diurnal

313   variations of SOC, POC and HO$_2$.

314

315   Among the elements, K (2060.7 $\pm$ 82.3 ng/m^3), Fe (996.5 $\pm$ 34.3 ng/m^3) and Ca (774.1 $\pm$ 39.4

316   ng/m^3) were the most abundant species, accounting for 47.0 $\pm$ 2.2%, 21.4 $\pm$ 0.3% and 15.6 $\pm$

317   0.3% of the total analyzed elements, respectively. Inconsistent with many other studies (Lyu

318   et al., 2015a; Cao et al., 2012) which reported the highest concentrations of crustal elements,

319   the highest K indicated the significance of biomass burning in or around Wuhan during the

320   monitoring period, because K is a tracer of biomass burning (Saarikoski et al., 2007; Echalar

321   et al., 1995).

322

323   **3.2.2 Comparison between episodes and non-episodes**

324   The concentrations of PM$_{2.5}$ components all increased significantly during the episodes

325   (Figure 3). Figure 7 presents chemical composition of PM$_{2.5}$ during episodes and

326   non-episodes in summer and autumn. Since WSIs data were not available in summer, the

327   proportions of the components were relative to the total mass resolved in PM$_{2.5}$ for cases 1-3

328   and non-episode 1. In summer, the fraction of OC decreased significantly ($p<0.05$) from the

329   non-episode 1 (57.3 $\pm$ 0.9%) to the episodes (53.0 $\pm$ 1.1%, 48.3 $\pm$ 2.6% and 55.4 $\pm$ 1.1% for

330   case 1, case 2 and case 3, respectively), indicating that the increment of OC was not the main

331   cause of the summer episodes. Conversely, the proportion of EC was significantly higher in

332   case 1 (19.5 $\pm$ 1.1%) (0.05$<p<$0.1, single tailed) and case 3 (22.0 $\pm$ 0.7%) ($p<0.05$, two tailed)

333   than that in non-episode 1 (18.7 $\pm$ 0.8%). EC was generally the tracer of incomplete

334   combustion (Chow et al., 1996). The accumulation of EC in PM$_{2.5}$ in case 1 and case 3

335   implied the enhancement of combustion source, *e.g.*, biomass burning. Furthermore, as the

336   indicator of biomass burning (Saarikoski et al., 2007; Echalar et al., 1995), K was remarkably

337   enhanced during the episodes, with the proportion in PM$_{2.5}$ increased from 8.5 $\pm$ 0.3% in

338   non-episode 1 to 16.1 $\pm$ 1.0% in case 1and 11.9 $\pm$ 0.3% in case 3, suggesting that biomass

339   burning was the leading factor of case 1 and case 3. However, consistent with that of OC, the

340   proportion of EC reduced to 15.0 $\pm$ 1.5% in case 2, which was just opposite to the increase of

341   the proportions of Ca (4.8$\pm$0.4% in non-episode 1 and 11.0 $\pm$ 1.9% in case 2) and Fe (6.3$\pm$0.3%

Atmospheric
Chemistry
and Physics
Discussions

342   in non-episode 1 and 10.1 $\pm$ 1.2% in case 2). Since Ca and Fe were generally originated from

343   the crust dust, the opposite behavior of OC/EC to Ca/Fe indicated that fugitive dust rather

344   than combustion source led to the occurrence of case 2. It is noteworthy that the proportion of

345   K in case 2 (11.6 $\pm$ 0.7%) was also higher than that in non-episode 1 (8.5 $\pm$ 0.3%; $p<0.05$),

346   suggesting that biomass burning also made some contribution to the increment of $PM_{2.5}$ in

347   case 2.

348   In autumn, the proportion of secondary inorganic ions decreased significantly ($p<0.05$) from

349   non-episode 2 (70.9 $\pm$ 0.9%) to case 4 (62.3 $\pm$ 0.8%) and case 5 (67.0 $\pm$ 0.8%), suggesting

350   that the case 4 and case 5 were not directly caused by the increment of SIOA. In case 6, the

351   proportion of secondary inorganic ions slightly decreased to 69.3 $\pm$ 1.1%, while the content of

352   NO_3^- substantially increased to 26.1 $\pm$ 1.0% from 19.8 $\pm$ 0.9% in non-episode 2. The causes

353   of soaring NO_3^- were discussed in section 3.4.2. For the proportion of OC, it increased from

354   20.9 $\pm$ 0.8% in non-episode 2 to 27.3 $\pm$ 0.7% in case 4, 23.8 $\pm$ 1.5% in case 5 and 21.5 $\pm$ 0.8%

355   in case 6. Consistently, the concentrations of EC and K also increased during the episodes,

356   although there was no significance for the increments ($p>0.05$). To conclude, the

357   enhancement of NO_3^- (only for case 6) and OC were the main causes of the autumn episodes,

358   which might be attributable to the biomass burning.
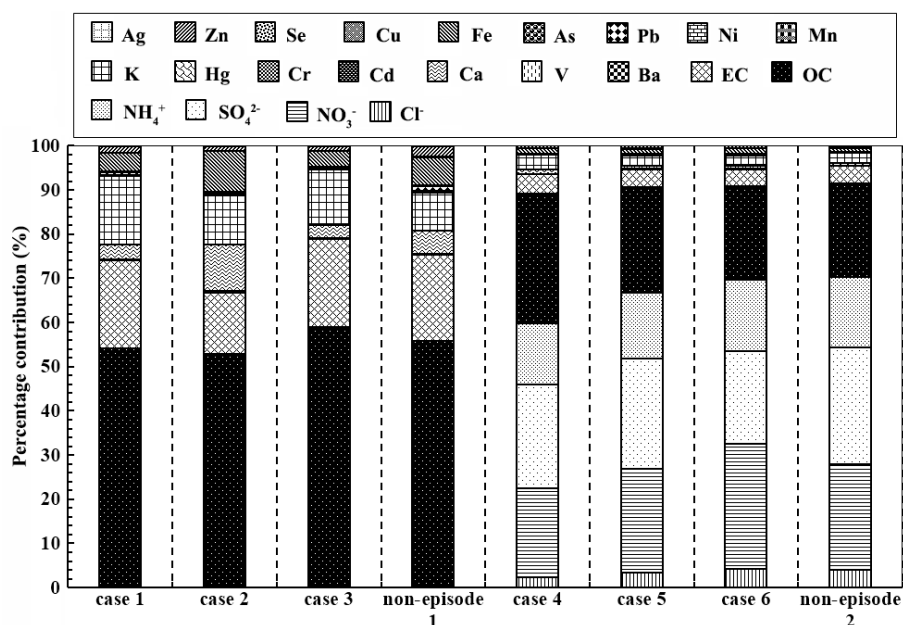
359

360   Figure 7 Chemical composition of PM$_{2.5}$ during episodes and non-episodes in summer and autumn

361

362   **3.3 Causes of PM$_{2.5}$ episodes**

363   **3.3.1 Meteorological conditions**

364   The processes of particle formation, dispersion and deposition were closely related to the

365   meteorological conditions. To interpret the possible causes of the PM$_{2.5}$ episodes, Figure 8

366   shows the patterns of wind direction/speed, temperature, relative humidity and pressure in

367   Wuhan during the monitoring period. Generally, the southeast winds prevailed at the

368   sampling site, with the wind speed of approximately 1.0 m/s. The low wind speed indicated

369   the dominance of local air masses. However, due to the high stability and long lifetime of

370   PM$_{2.5}$, the regional/superregional impact couldn't be eliminated. In comparison with those in

371   summer, the wind speed (summer: 1.1 $\pm$ 0.04 m/s; autumn: 0.8 $\pm$ 0.03 m/s) and temperature

372   (summer: 25.6 $\pm$ 0.2 m/s; autumn: 17.5 $\pm$ 0.3 m/s) were significantly ($p<0.05$) lower in

373   autumn, while the pressure (summer: 1006.9 $\pm$ 0.2 hPa; autumn: 1020.9 $\pm$ 0.2 hPa) was much

374   higher. During the episodes, the wind speed was generally lower than those in non-episodes

375   except for case 5. This might be one cause for the episodes, but it couldn't fully explain the

376   great enhancements of PM$_{2.5}$, because the wind speeds were very low and their differences

377   between the episodes and non-episodes were minor. Furthermore, the pressure was not very

378   high during the episodes except for case 6, suggesting that the synoptic system was not

379   responsible for the occurrence of PM$_{2.5}$ episodes.

380

381   Figure 8 Meteorological patterns in Wuhan during the monitoring period. The red-highlighted areas

382   represent PM$_{2.5}$ episodes.

Atmospheric
Chemistry
and Physics
Discussions
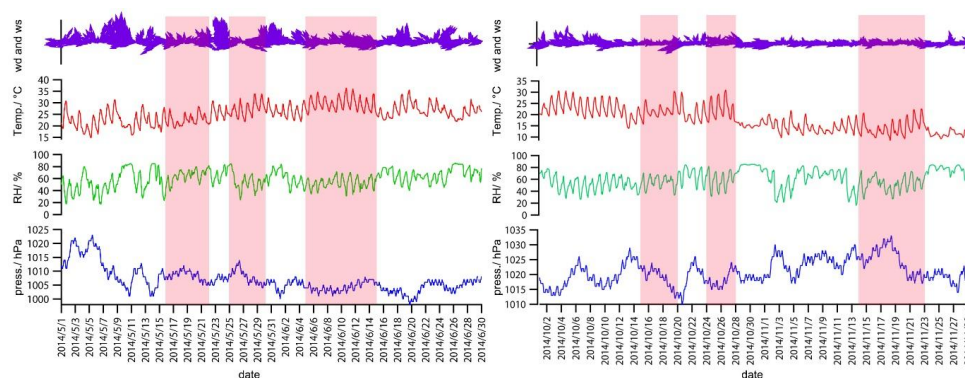
3.3.2 Signatures of chemical tracers

Figure 9 compares the levels of some tracer species between the episodes and non-episodes. Due to the differences in meteorological conditions and background levels, the comparisons were conducted between the episodes and non-episodes in the same season. Noticeably, the tracers of biomass burning (*i.e.*, C_2H_2, CH_3Cl, CH_3CN and K) (Guo et al., 2011b; Simoneit, 2002) were much enhanced during the episodes, compared to those in non-episodes. An exception was the insignificant increment of CH_3Cl in case 6, when 70% data were not available due to the instrumental error. In general, the higher levels of C_2H_2, CH_3Cl, CH_3CN and K during the episodes suggested the leading role of biomass burning in building up $PM_{2.5}$. Furthermore, OC and EC also increased substantially during the episodes, consistent with the findings of previous studies (Agarwal, et al., 2010; Duan et al., 2004) that biomass burning led to great increment of the carbonaceous aerosols.

It is noteworthy that the concentrations of Ca and Fe were the most outstanding in case 2, suggesting that the fugitive dust was an important contributor to $PM_{2.5}$ in case 2, in addition to biomass burning.
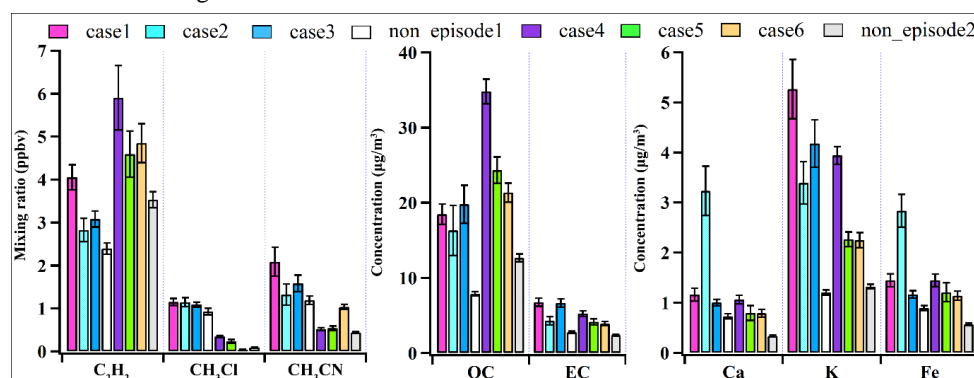
Figure 9 Concentrations of tracer species during $PM_{2.5}$ episodes and non-episodes

### 3.3.3 Source apportionment

To clarify the sources of $PM_{2.5}$ and quantify their contributions, the hourly observation data of $PM_{2.5}$ components were applied to PMF for source apportionment. Due to the lack of WSIs in May and June, the results in summer were only applicable to the sum of the resolved species in $PM_{2.5}$. Under the principle of lowest Q value, the simulations which best

Atmospheric
Chemistry
and Physics
Discussions

Open Access

406   reproduced the observed concentrations of all the species were selected. Figure 10 and Figure

407   11 present the source profiles in summer and autumn, respectively. The profiles were quite

408   similar in different scenarios, and four factors were resolved. Factor 1 had high loadings of

409   the crust elements (*i.e.*, Ba, Ca, Mn and Fe), indicating the source of fugitive dust. Factor 2

410   was likely associated with oil refinery and usage, in view of the high percentages of V and Ni,

411   which often originated from the combustion of heavy oil (Barwise et al., 1990; Nriagu and

412   Pacyna, 1988). Factor 3 was distinguished by the high loadings of Pb, Cu, Se and As,

413   generally indicating the coal combustion (Querol et al., 1995). Finally, OC, EC and secondary

414   inorganic ions were highly accumulated in the last factor, with the dominance of biomass

415   burning tracers (*i.e.*, K and Hg) (Zhang et al., 2013; Friedli et al., 2003). As such, this factor

416   was assigned as biomass burning.

417   Table 3 summarizes the mass concentrations and percentage contributions of each source to

418   the sum of resolved species in $PM_{2.5}$. Generally, biomass burning made the greatest

419   contribution to the total mass of $PM_{2.5}$ components (from 37.3 $\pm$ 3.7% in case 2 to 70.1 $\pm$ 0.5%

420   in case 3), followed by coal combustion (from 18.5 $\pm$ 0.9% in case 3 to 44.9 $\pm$ 1.7% in

421   non-episode 2), oil refinery/ usage (from 7.9 $\pm$ 0.3% in case 2 to 24.4 $\pm$ 1.4% in case 5) and

422   fugitive dust (from 2.2 $\pm$ 1.0% in non-episode 2 to 17.6 $\pm$ 1.2% in case 2). Noticeably, in

423   comparison with that during non-episodes, the contributions of biomass burning were

424   significantly higher during the episodes, while the other sources remained relatively stable,

425   except for case 2 and case 5. This confirmed that biomass burning was the leading factor for

426   cases 1, 3, 4 and 6. In case 2, the contributions of fugitive dust (5.0 $\pm$ 0.3 $\mu g/m^3$, 17.6 $\pm$ 1.2%)

427   and oil refinery/usage (6.9 $\pm$ 0.8 $\mu g/m^3$, 24.3 $\pm$ 2.9%) increased considerably compared to

428   those in non-episode 1 (1.2 $\pm$ 0.1 $\mu g/m^3$, 9.8 $\pm$ 0.9% and 2.4 $\pm$ 0.1 $\mu g/m^3$, 7.9 $\pm$ 0.3% for

429   fugitive dust and oil refinery/usage, respectively). However, the percentage contribution of

430   biomass burning decreased to 37.3 $\pm$ 3.7% from 41.0 $\pm$ 0.9% in non-episode 1. The variation

431   of source contributions suggested that fugitive dust and oil refinery/usage were the main

432   causes of case 2. Relative to source contributions in non-episode 2, the contribution of oil

433   refinery/usage in case 5 also increased by 15.1 $\pm$ 2.6 $\mu g/m^3$, in addition to the enhancement of

434   biomass burning (21.8 $\pm$ 1.7 $\mu g/m^3$), revealing the combined effect of oil refinery/usage and

435   biomass burning on case 5.

436
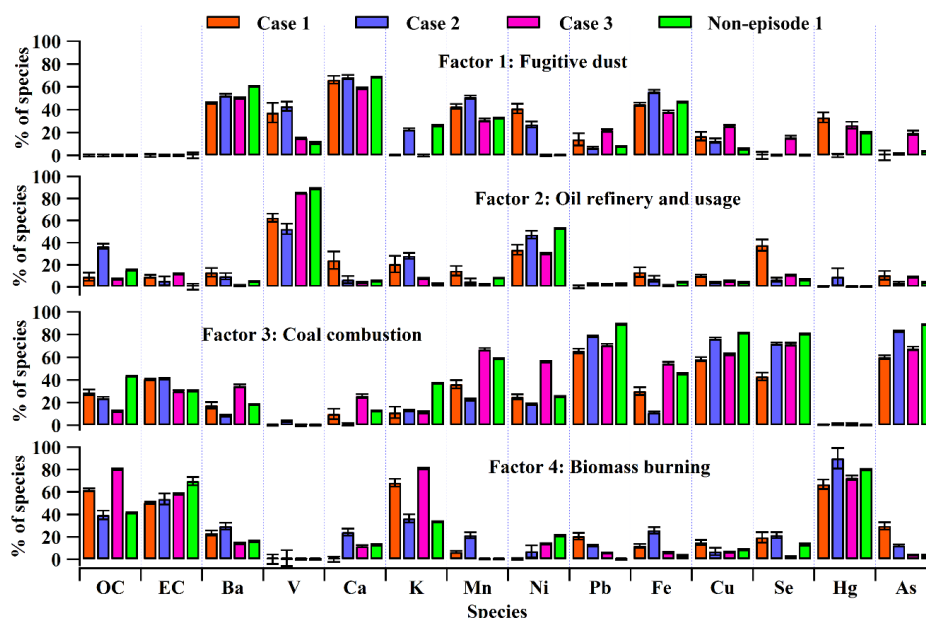
Figure 10 Profiles of the PM$_{2.5}$ sources in summer
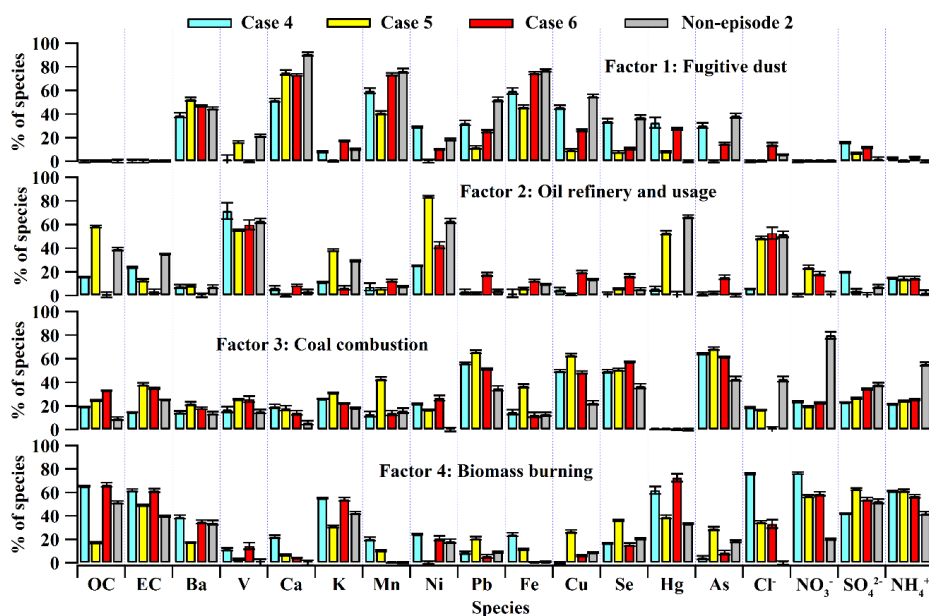
438

439   Figure 11 Profiles of the PM$_{2.5}$ sources in autumn

440

441

Atmospheric
Chemistry
and Physics
Discussions

Open Access

EGU

442   Table 3 Mass concentration ($\mu g/m^3$) and percentage contribution (shown in the bracket, %) of the

443   sources to the sum of the resolved species in $PM_{2.5}$

|	Fugitive dust	Oil refinery and usage	Coal combustion	Biomass burning
Case 1	1.5 ±0.3	3.5 ±1.3	8.4 ±0.8	**16.6 ±0.5**
	(5.0 ±1.1)	(11.6 ±4.1)	(27.9 ±2.6)	**(55.4 ±1.6)**
Case 2	**5.0 ±0.3**	**6.9 ±0.8**	6.0 ±0.3	10.6 ±1.1
	(17.6 ±1.2)	**(24.3 ±2.9)**	(20.9 ±1.0)	(37.3 ±3.7)
Case 3	1.1 ±0.2	2.4 ±0.1	5.6 ±0.3	**21.1 ±0.2**
	(3.5 ±0.8)	(7.9 ±0.3)	(18.5 ±0.9)	**(70.1 ±0.5)**
Non-episode 1	1.2 ±0.1	1.2 ±0.1	4.7 ±0.03	4.9 ±0.1
	(9.8 ±0.9)	(9.7 ±1.0)	(39.5 ±0.2)	(41.0 ±0.9)
Case 4	6.5 ± 1.1	14.7 ±0.8	24.0 ±0.5	**67.7 ±0.7**
	(5.8 ±0.9)	(13.0 ±0.7)	(21.3 ±0.4)	**(59.9 ±0.6)**
Case 5	2.8 ±0.7	**23.1 ±1.4**	23.3 ±0.6	**45.4 ±0.9**
	(3.0 ±0.7)	**(24.4 ±1.4)**	(24.6 ±0.7)	**(48.0 ±1.0)**
Case 6	5.2 ±0.7	10.0 ±2.0	26.2 ±0.6	**54.8 ±1.7**
	(5.4 ±0.7)	(10.4 ±2.1)	(27.2 ±0.7)	**(56.9 ±1.7)**
Non-episode 2	1.3 ±0.6	8.0 ±1.2	26.8 ±1.0	23.6 ±0.8
	(2.2 ±1.0)	(13.4 ±1.9)	(44.9 ±1.7)	(39.5 ±1.3)

444

445   **3.3.4 Open fires and air mass trajectories**

446   To further confirm the biomass burning activities during the $PM_{2.5}$ episodes, the fire spot

447   distribution (downloaded from NASA Firms Web Fire Mapper, and accessible at

448   https://firms.modaps.eosdis.nasa.gov/firemap/) and 72-h backward air mass trajectories

449   (simulated by Hysplit v4.9 model) are plotted in Figure 12. Noticeably, the air masses

450   arriving in Wuhan had passed over the areas where the open fires were detected. In case 2,

451   the air mass trajectories were mainly from the south and northwest and evaded the intensive

452   burning areas in northeast China, which might explain why biomass burning was not a

453 predominant factor in case 2. In contrast, the fire spots were extremely dense in case 3 in

454 northeast China where the air masses originated or passed over, corresponding to the highest

455 contribution of biomass burning to the sum of $PM_{2.5}$ components (70.1 $\pm$0.5%). Please note,

456 the fire spot distribution resolved by satellite was also influenced by meteorological

457 conditions. For example, the open fires were seldom observed along the air mass trajectories

458 in case 6, which was contradictory to the source apportionment result in which biomass

459 burning was the leading factor to this episode with the contribution of 56.9 $\pm$1.7%. However,

460 the satellite observations revealed that the cloud cover was the highest reaching 80% in case

461 6 (*i.e.*, 8.0 as shown in Figure 12). This likely caused the discrepancy between the fire spot

462 distribution and the source apportionment. Furthermore, the temperature in case 6 (14.9 $\pm$0.5

463 ℃) was significantly lower than that in other cases (*p*<0.05), which might strengthen the

464 main causes of $PM_{2.5}$ pollution (*i.e.*, biomass burning), because the gas-to-particle conversion

465 was preferable at low temperature, such as the NO_3^- formation discussed in section 3.4.2.
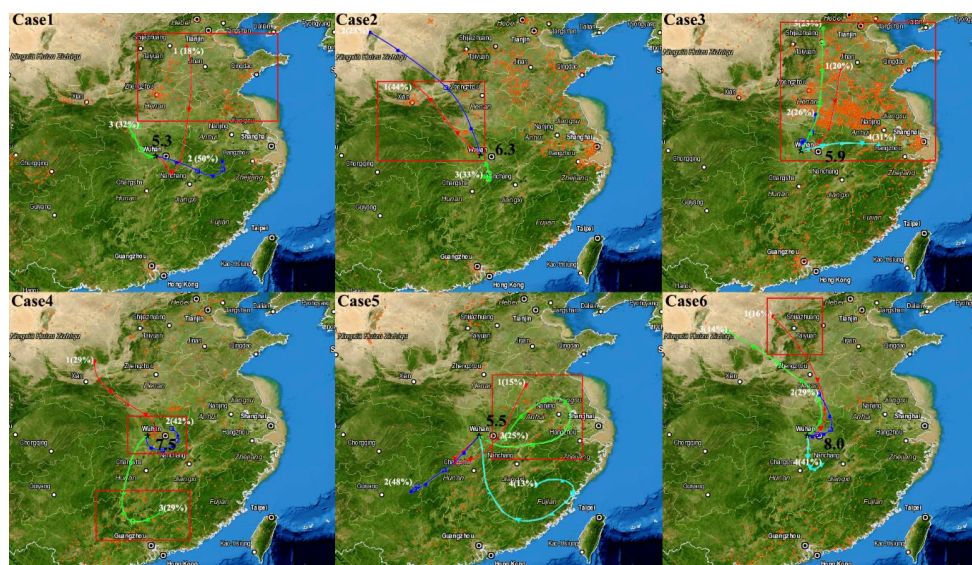
467 Figure 12 Fire spot distribution and 72-h backward air mass trajectories. The red squares demonstrate

468 the potential areas where the biomass burning aggravated particulate pollution in Wuhan. The black

469 figures in each case refer to the average cloud cover.

3.4 Formation mechanisms

Atmospheric
Chemistry
and Physics
Discussions

3.4.1 Model validation

In this study, the PBM-MCM model was used to help investigate the formation mechanisms

of NO_3^- and SOC. Prior to the application, the model was validated through the test of O_3

simulation. Figure 13 compares the daily averages and diurnal variations of O_3 between the

simulation and observation. It was found that the model well simulated O_3 variation in both

daily and diurnal patterns. However, it generally overestimated the O_3 levels in November.

The meteorological parameters indicated that the frequency of foggy days was extremely

high (36.7%) in November, possibly resulting in the weakening of solar radiation and

photochemical reactivity consequently. To quantitatively evaluate the performance of the

model, the index of agreement (IOA) was calculated using Equation 9.
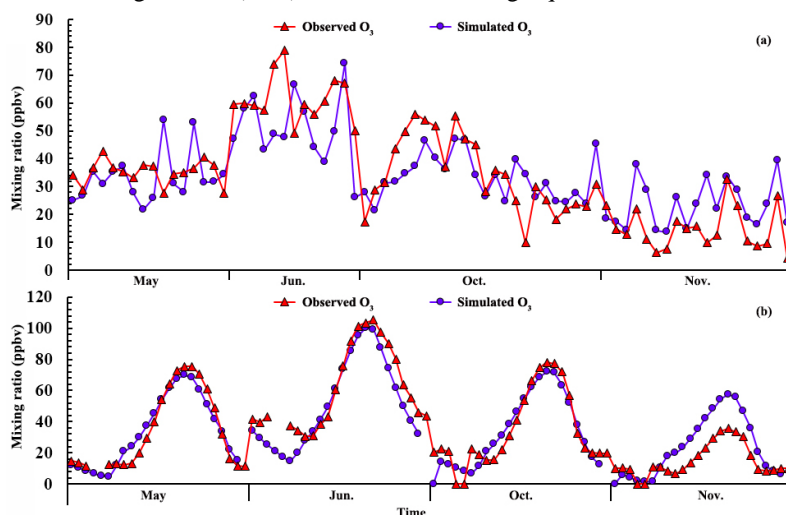
Figure 12 Comparisons of the (a) daily and (b) diurnal O_3 between simulation and observation. Rainy

days were excluded.

$$IOA = 1 - \frac{\sum_{i=1}^{n}(O_i - S_i)^2}{\sum_{i=1}^{n}(|O_i - \bar{O}| + |S_i - \bar{O}|)^2} \quad (Eq.9)$$

where $\bar{O}$ was the average of n samples, and O_i and S_i represented the observed and

simulated values, respectively. Within the interval of [0, 1], Higher IOA value indicated better

agreement between the simulation and observation.

By calculation, IOA reached 0.86, indicating the excellent performance of the model in O_3

simulation. Since O_3 production is tightly associated with the oxidative radicals,

22

492   intermediates and products, the robust O_3 simulation gave us full confidence to accept the

493   simulated N_2O_5, HO_2, SVOCs, etc.

494

495   **3.4.2 NO_3^- formation**

496   The composition analysis indicated that the proportion of NO_3^- increased remarkably in case

497   6. To interpret this phenomenon, the formation mechanisms of NO_3^- were investigated. Figure

498   14 shows the hourly variations of the calculated and observed NO_3^- and the contribution of

499   R3 (*i.e.*, $N_2O_5 + H_2O \rightarrow 2HNO_3$), among which $NO_{3\ cal\ 1}^-$, $NO_{3\ cal\ 2}^-$ and $NO_{3\ obs}^-$ referred to

500   homogeneous formation (R1 and R2), total formation (R1, R2 and R3) and field

501   measurement of NO_3^-, respectively. Although the particle-bound NO_3^- was influenced by

502   many factors (*i.e.*, formation, deposition and dispersion), the calculations generally well

503   reproduced the measured NO_3^- in case 6, with high correlation coefficient ($R^2 = 0.63$) and IOA

504   of 0.78. However, on November 23, 2014, the observed NO_3^- decreased rapidly from 09:00,

505   which was not captured by the calculations. This discrepancy was likely caused by the

506   weather conditions on that day, because (1) the average wind speed increased from 1.7 m/s

507   before 09:00 to 2.7 m/s after 09:00 and even reached 4.0 m/s at 14:00; and (2) the moderate

508   rain began at 12:00 and continued to 23:00, with the total precipitation of 24 mm. Indeed, this

509   was the beginning of a 7-day rainy period, which ended case 6 with a sharp decrease of $PM_{2.5}$

510   concentration (approximately 175 µg/m^3) (see Figure 2).

511   As the values of $NO_{3\ cal\ 1}^-$ were very close to $NO_{3\ cal\ 2}^-$, the variation of NO_3^- in case 6 could be

512   well explained by the homogeneous formation (R1 and R2), while the heterogeneous reaction

513   of N_2O_5 on aerosol surfaces (R3) only made minor contribution to the total NO_3^- (*i.e.*, nearly

514   nil during 0:00-17:00, and $3.7 \pm 0.6\%$ during 18:00-23:00). Since the homogeneous

515   formation of NO_3^- was closely related to the concentrations of HNO_3 (g) and NH_3 (g), and

516   temperature (see R1 and R2), Table 4 compares the temperature, HNO_3 (g), NH_3 (g), NO,

517   NO_2, O_3, and the simulated OH and HO_2 (a measure of oxidative capacity (Cheng et al.,

518   2010)) between case 6 and non-episode 2. It was found that HNO_3 (g) (0.65 ± 0.01 ppbv) and

519   NH_3 (g) (13.48 ± 0.72 ppbv) in case 6 were significantly higher than those during the

520   non-episode 2 (0.47 ± 0.03 and 9.54 ± 0.37 ppbv for HNO_3 and NH_3, respectively), which

521   might substantially favor the formation of NH_4NO_3. As HNO_3 (g) was generally formed

Atmospheric
Chemistry
and Physics
Discussions

522   through the oxidation of NO_x, the production of HNO_3 (g) should be closely related to the

523   oxidative capacity of the air and the level of NO_x. In case 6, O_3 (17.09 $\pm$ 2.04 ppbv), OH ((3.8

524   $\pm$ 1.3) $\times$ 10^5 molecules/cm^3) and HO_2 ((1.1 $\pm$ 0.3) $\times$ 10^7 molecules/cm^3) were noticeably

525   lower than those in non-episode 2 (O_3: 24.57 $\pm$ 1.64 ppbv; OH: (7.2 $\pm$ 0.9) $\times$ 10^5

526   molecules/cm^3; HO_2: (2.0 $\pm$ 0.2) $\times$ 10^7 molecules/cm^3), indicating the weaker oxidative

527   capacity. However, NO (43.55 $\pm$ 11.65 ppbv) and NO_2 (44.93 $\pm$ 2.29 ppbv) were much higher

528   as compared to those in non-episode 2 (14.70 $\pm$ 2.40 and 29.46 $\pm$ 0.95 ppbv for NO and NO_2,

529   respectively), possibly leading to the enhancement of HNO_3 (g) in case 6. Furthermore, the

530   particle-bound NO_3^- was of low thermal stability (Querol et al., 2004), and the temperature

531   lowered ~2.3 C° in case 6, which suppressed the decomposition and volatilization of

532   NH_4NO_3. Therefore, the high levels of NO_x and NH_3, and low temperature were both

533   responsible for the NO_3^- increment in case 6.
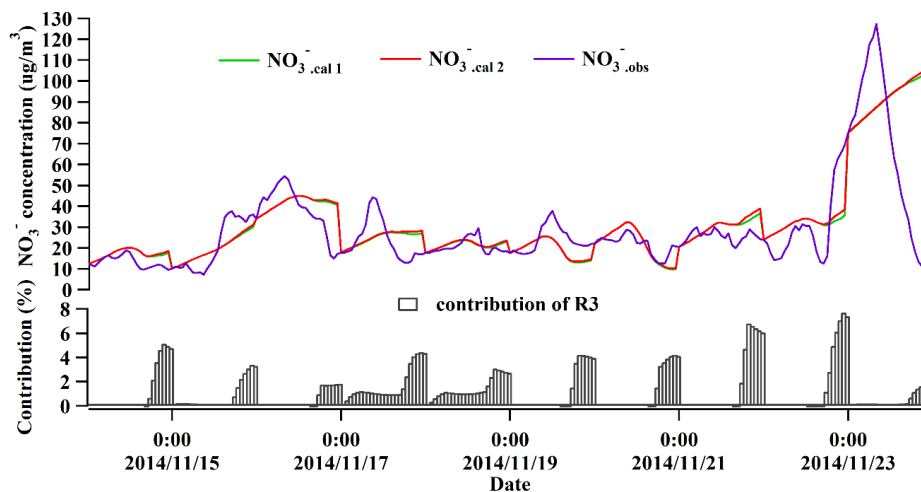
Figure 14 Comparison of NO_3^- between the theoretical calculations and observation in case 6

Table 4 Comparison of temperature, HNO_3 (g), NH_3 (g), NO, NO_2, O_3 and simulated OH and HO_2

between case 6 and non-episode 2

	Case 6	Non-episode 2
Temperature (C°)	14.9 $\pm$ 0.5	17.2 $\pm$ 0.3
HNO_3 (ppbv)	0.65 $\pm$ 0.01	0.47 $\pm$ 0.03

Atmospheric
Chemistry
and Physics
Discussions

NH_3 (ppbv)	13.48 ± 0.72	9.54 ± 0.37
NO (ppbv)	43.55 ± 11.65	14.70 ± 2.40
NO_2 (ppbv)	44.93 ± 2.29	29.46 ± 0.95
O_3 (ppbv)	17.09 ± 2.04	24.57 ± 1.64
OH (molecules/cm^3)	$(3.8 \pm 1.3) \times 10^5$	$(7.2 \pm 0.9) \times 10^5$
HO_2 (molecules/cm^3)	$(1.1 \pm 0.3) \times 10^7$	$(2.0 \pm 0.2) \times 10^7$

539

540   **3.4.3 SOC formation**

541   Apart from high NO_3^- in case 6, the proportions of OC also increased during the autumn

542   episodes. Since SOC is an important fraction in OC, and it often grows with the aging of air

543   mass, it could be of help to explain the increase of OC in autumn episodes by exploring the

544   possible formation mechanisms of SOC. It is well known that SOC formation is closely

545   related to semi-volatile oxidation products of VOCs (SVOCs), which are formed from the

546   reactions between oxidative radicals (*i.e.*, RO_2 and HO_2) (Kanakidou et al., 2005; Forstner et

547   al., 1997). Hence, the relationship between SOC and SVOCs was investigated. It should be

548   noted that the SVOCs were simulated by the PBM-MCM model, and SOC was calculated

549   with the EC-tracer method mentioned in section 3.2.1. The speciation of SVOCs and their

550   precursors can be found in the supplementary material Table S1. Briefly, the precursors of

551   SVOCs include isoprene, aromatics and C_7-C_{12} n-alkanes.

552   Figure 15 presents daily and diurnal variations of SOC and SVOCs. It was found that SOC

553   correlated well with SVOCs in both daily (R^2=0.52) and diurnal (R^2=0.63) patterns in autumn,

554   indicating that the simulated SVOCs were responsible for the production of SOC. The

555   oxidation products of aromatics and isoprene were the main constituents of the SVOCs, with

556   the average contribution of $42.5 \pm 2.8\%$ and $39.4 \pm 2.0\%$, respectively. Among the aromatics,

557   xylenes made the greatest contribution ($15.0 \pm 0.7\%$) to the SVOCs, followed by

558   trimethylbenzenes ($11.5 \pm 0.7\%$), ethylbenzene ($8.8 \pm 0.5\%$), toluene ($5.1 \pm 0.7\%$) and

559   benzene ($2.2 \pm 0.2\%$). Compared to those in non-episode 2 (*i.e.*, $40.7 \pm 3.4\%$ and $41.1 \pm 2.4\%$

560   contributed by the aromatics and isoprene, respectively), the contribution of aromatics to

561   SVOCs increased to $46.3 \pm 4.1\%$ during the episodes, while the proportion of the isoprene

Atmospheric
Chemistry
and Physics
Discussions

562 oxidation products decreased to 36.1 ± 3.7%, suggesting that the increment of aromatics was

563 the main cause of the autumn episodes. To quantify the contribution of biomass burning to

564 SOC, the observed VOCs were apportioned to different sources, including biomass burning

565 with CH_3CN as the tracer. The source profiles were provided in the supplementary material

566 Figure S2. According to the SVOCs simulated on the basis of VOCs emitted from biomass

567 burning, the SVOCs was elevated by 15.4 ± 1.3% due to the biomass burning during the

568 episodes.

569 In contrast, the correlations were much worse in summer (R^2= 0.01 and 0.31 for daily and

570 diurnal variations, respectively). The high frequency (50.8%) of rainy days in summer was a

571 factor for the poor correlation, *e.g.*, SOC was pretty low during the late period of June when

572 the precipitation lasted for about 10 days, while the model overestimated the SVOCs without

573 considering the influence of precipitation. The correlations between SOC and SVOCs (R^2=

574 0.14 and 0.19 for the daily and diurnal variations, respectively) were still poor after the rainy

575 days were excluded. Hence, the poor correlation should also relate to other factors such as

576 incomplete consideration of the contribution of biogenic VOCs. Although isoprene was

577 included as a precursor of the SVOCs, the other biogenic species (*i.e.*, α-pinene, β-pinene and

578 monoterpenes) were not monitored in this study, which were proven as important precursors

579 of SOC (Kanakidou et al., 2005). Moreover, the level of biogenic VOCs was much higher in

580 summer than that in autumn. Taking isoprene as an example, the mixing ratio of isoprene was

581 66.7 ± 4.9 pptv in summer and only 37.2 ± 2.6 pptv in autumn. The higher missing level of

582 biogenic VOCs in summer led to a higher deficit of SVOCs, perhaps causing the poorer

583 correlation between SOC and SVOCs. Nevertheless, this needs further validation with more

584 comprehensive data of biogenic VOCs.

Atmospheric
Chemistry
and Physics
Discussions

Open Access
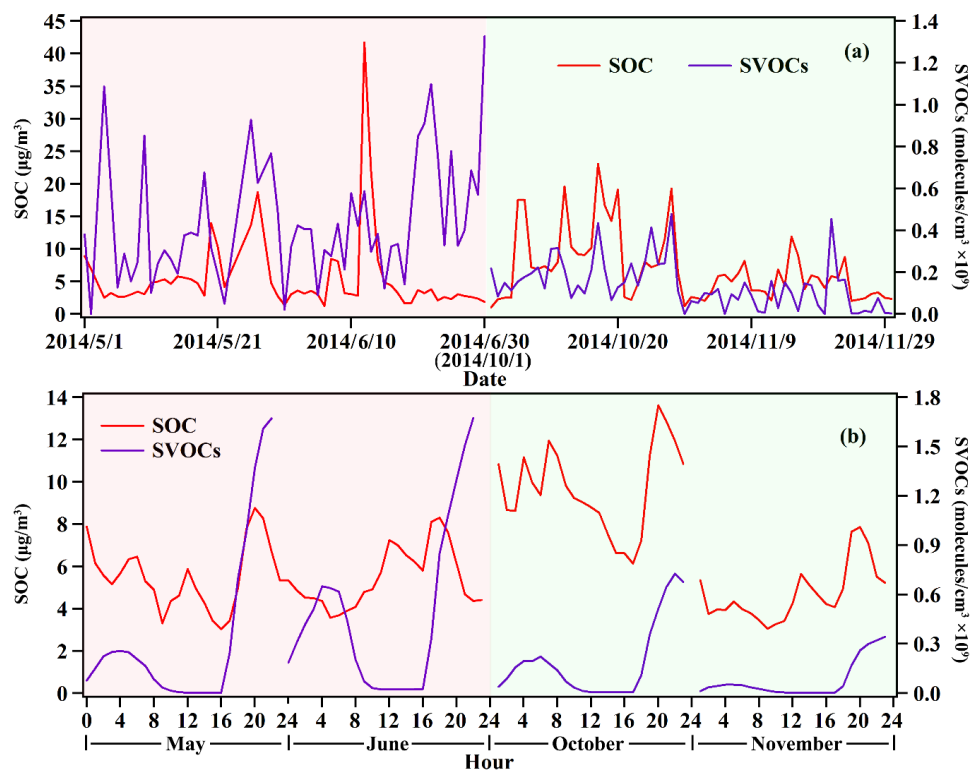
Figure 14 (a) Daily and (b) diurnal variations of SOC and SVOCs. The red and green highlighted

areas represent the summer and autumn period, respectively.

4. Conclusions

In summer and autumn 2014, the concentrations of $PM_{2.5}$ and its components were
continuously monitored in Wuhan, among which six $PM_{2.5}$ episodes were captured. The
analysis of $PM_{2.5}$ concentration and compositions found that Wuhan suffered from relatively
high level of $PM_{2.5}$, even in the warm seasons. Secondary inorganic ions were the most
predominant species in $PM_{2.5}$ in the form of NH_4NO_3 and $(NH_4)_2SO_4$. The comparable levels
of SO_4^{2-} and NO_3^- indicated that stationary and mobile sources were equivalently important in
Wuhan. With the EC-tracer method, it was found that POC was slightly higher than SOC, and
they both increased significantly during the episodes. K was the most abundant element,
implying the biomass burning in/around Wuhan during the sampling campaign. Indeed, the
source apportionment revealed that biomass burning was the greatest contributor to $PM_{2.5}$

Atmospheric
Chemistry
and Physics
Discussions

600 during the episodes except for case 2. Fugitive dust and oil refinery/usage were the main

601 causes of case 2. Study of the formation mechanism of NO_3^- and SOC found that NO_3^- was

602 mainly generated from the homogeneous reactions in case 6, and the high levels of NO_x and

603 NH_3, and the low temperature caused the increment of NO_3^-. Furthermore, the daily and

604 diurnal variations of SOC correlated well with those of SVOCs in autumn. The aromatics and

605 isoprene were the main precursors of SOC, and the contribution of aromatics increased

606 during the episodes. However, the correlation between SOC and SVOCs was much worse in

607 summer, possibly resulting from the incompleteness of biogenic VOCs input in simulating

608 the SVOCs. This study provided comprehensive knowledge on the chemical characteristics of

609 $PM_{2.5}$ in warm seasons in Wuhan, and for the first time quantified the contribution of biomass

610 burning to $PM_{2.5}$. The investigation of SOC formation will also inspire the application of the

611 explicit chemical mechanisms on the study of SOA.

612

618

619 **References**

620 Agarwal, S., Aggarwal, S.G., Okuzawa, K., and Kawamura, K., 2010: Size distributions of

621   dicarboxylic acids, ketoacids, α-dicarbonyls, sugars, WSOC, OC, EC and inorganic ions in

622   atmospheric particles over Northern Japan: implication for long-range transport of Siberian

623   biomass burning and East Asian polluted aerosols. Atmos. Chem. Phys. 10, 5839-5858.

624 Anderson, J.O., Thundiyil, J.G., and Stolbach, A., 2012: Clearing the air: A review of the effects of

625   particulate matter air pollution on human health. J. Med. Toxicol. 8, 166-175.

626 Arimoto, R., Duce, R.A., Savoie, D.L., Prospero, J.M., Talbot, R., Cullen, J.D., Tomaza, U., Lewis,

627   N.F., and Ray, B.J., 1996: Relationships among aerosol constituents from Asia and the North

628   Pacific during PEM-West A. J. Geophys. Res. 101, 2011-2023.

629 Aumont, B., Madronich, S., Ammann, M., Kalberer, M., Baltnesperger, U., Hauglustaine, D.,

Atmospheric
Chemistry
and Physics
Discussions

630   Baltensperger, F., 1999: On the NO_2 + soot reaction in the atmosphere. J. Geophys. Res. 104,

631   1729-1736.

632   Barwise, A.J.G., 1990: Role of Nickel and Vanadium in petroleum classification. Energy & Fuels 4,

633   647-652.

634   Brown, S.G., Frankel, A., and Hafner, H.R.: Source apportionment of VOCs in Los Angeles area using

635   positive matrix factorization, Atmos. Environ. 41, 227-237, 2007.

636   Cao, J.J., Shen, Z.X., Chow, J.C., Watson, J.G., Lee, S.C., Tie, X.X., Ho, K.F., Wang, G.H., and Han,

637   Y.M., 2012: Winter and summer $PM_{2.5}$ chemical compositions in fourteen Chinese cities. J Air

638   Waste Manage. Assoc. 62, 1214-1226.

639   Cao, J.J., Wu, F., Chow, J.C., Lee, S.C, Li, Y., Chen, S.W., An, Z.S., Fung, K.K., Watson, J.G., Zhu, C.S.,

640   and Liu, S.X., 2005: Characterization and source apportionment of atmospheric organic and elemental

641   carbon during fall and winter of 2003 in Xi'an, China. Atmos. Chem. Phys. 5, 3127-3137.

642   Cheng, H.R., Gong, W., Wang, Z.W., Zhang, F., Wang, X.M., Lv, X.P., Liu, J., Fu, X.X., Zhang, G., 2014:

643   Ionic composition of submicron particles ($PM_{1.0}$) during the long-lasting haze period in January 2013 in

644   Wuhan, central China. J. Environ. Sci. 26(4), 810-817.

645   Cheng, H.R., Guo, H., Wang, X.M., Saunders, S.M., Lam, S.H.M., Jiang, F., Wang, T.J., Ding, A.J., Lee,

646   S.C., and Ho, K.F., 2010: On the relationship between ozone and its precursors in the Pearl River Delta:

647   application of an observation-based model (OBM). Environ. Sci. Pollut. Res. 17, 547-560.

648   Chow, J.C, Watson, J.G., Lu, Z.Q., Lowenthal, D.H., Frazier, C.A., Solomon, P.A., Thuillier, R.H., and

649   Magliano, K., 1996: Descriptive analysis of $PM_{2.5}$ and PM_{10} at regionally representative locations

650   during SJVAQS/AUSPEX. Atmos. Environ. 30(12), 2079-2112.

651   Deng, X.J., Li, F., Li, Y.H., Li, J.Y., Huang, H.Z., Liu, X.T., 2015: Vertical distribution characteristics of

652   PM in the surface layer of Guangzhou. Particuology 20, 3-9.

653   Deng, X.J., Tie, X.X., Zhou, X.J., Wu, D., Zhong, L.J., Tan, H.B., Li, F., Huang, X.Y., Bi, X.Y., and Deng,

654   T., 2008: Effects of Southeast Asia biomass burning on aerosols and ozone concentrations over the Pearl

655   River Delta (PRD) region. Atmos. Environ. 43(36), 8493-8501.

656   Duan, F.K., He, K.B., Ma, Y.L., Jia, Y.T., Yang, F.M., Lei, Y., Tanaka, S., and Okuta, T., 2005:

657   Characteristics of carbonaceous aerosols in Beijing, China. Chemosphere 60(3), 355-364.

658   Duan, F.K., Liu, X.D., Yu, T., and Cachier, H., 2004: Identification and estimate of biomass burning

659   contribution to the urban aerosol organic carbon concentrations in Beijing. Atmos. Environ. 38(9),

660   1275-1282.

661   Echalar, F., Gaudichet, A., Cachier, H., and Artaxo, P., 1995: Aerosol emissions by tropical forest and

662   savanna biomass burning: characteristic trace elements and fluxes. Geophys. Res. Lett. 22, 3039-3042.

663   Forstner, H.J.L., Flagan, R.C., and Seinfeld, J.H., 1997: Secondary organic aerosol from the

664   photooxidation of aromatic hydrocarbons: molecular composition. Environ. Sci. Technol. 31 (5),

665   1345-1358.

666   Friedli, H.R., Radke, L.F., Lu, J.Y., Banic, C.M., Leaitch, W.R., and MacPherson, J.I., 2003: Mercury

667   emissions from burning of biomass from temperate North American forests: laboratory and airborne

668   measurements. Atmos. Environ. 37, 253-267.

669   GB 3095-2012, accessible from http://kjs.mep.gov.cn/ hjbhbz/ bzwb/ dqhjbh/ dqhjzlbz/ 201203/

670   W020120410330232398521.pdf.

671   Geng, F.H., Zhang, Q., Tie, X.X., Huang, M.Y., Ma, X.C., Deng, Z.Z., Yu, Q., Quan, J.N., and Zhao, C.S.,

672   2009: Aircraft measurements of O_3, NO_x, CO, VOCs, and SO_2 in the Yangtze River Delta region. Atmos.

673   Environ. 43, 584-593.

674   Goldberg, M.S., Burnett, R.T., Bailar III, J.C., Brook, J., Bonvalot, Y., Tamblyn, R., Singh, R., Valois, M.F.,

675   2001: The Association between Daily Mortality and Ambient Air Particle Pollution in Montreal, Quebec:

676   1. Nonaccidental Mortality. Environ. Res. 86(1), 12-25.

677   Gugamsetty, B., Wei, H., Liu, C.N., Awasthi, A., Hsu, S.C., Tsai, C.J, Roan, G.D., Wu, Y.C., and Chen,

678   C.F., 2012: Source Characterization and Apportionment of PM_{10}, $PM_{2.5}$ and $PM_{0.1}$ by Using Positive

679   Matrix Factorization. Aerosol Air Qual. Res. 12, 476-491.

680   Guo, H., Cheng, H.R., Ling, Z.H., Louie, P.K.K., and Ayoko, G.A., 2011b: Which emission sources are

681   responsible for the volatile organic compounds in the atmosphere of Pearl River Delta? J. Hazard. Mater.

682   188, 116-124.

683   Guo, H., Zou, S.C., Tsai, W.Y., Chan, L.Y., and Blake, D.R., 2011a: Emission characteristics of

684   nonmethane hydrocarbons from private cars and taxis at different driving speeds in Hong Kong. Atmos.

685   Environ. 45, 2711-2721.

686   Ho, K.F., Lee, S.C., Chan, C.K., Yu, J.C., Chow, J.C., Yao, X.H., 2003: Characterization of chemical

687   species in $PM_{2.5}$ and PM_{10} aerosols in Hong Kong. Atmos. Environ. 37(1), 31-39.

688   HKEPD, 2014. Air Quality in Hong Kong 2014, accessible at http://www.aqhi.gov.hk/en/download/air-

689   quality-reportse469.html?showall=&start=1.

690   Hu, J.H., and Abbatt, J.P.D., 1997: Reaction probabilities for N_2O_5 hydrolysis on sulfur acid and

691   ammonium sulfate aerosols at room temperature. J. Phys. Chem. 101A, 871-878.

692   Kanakidou, M., Seinfeld, J.H., Pandis, S.N., Barnes, I., Dentener, F.J., Facchini, M.C., Dingenen, R.V.,

693   Ervens, B., Nenes, A., Nielsen, C.J., Swietlicki, E., Putaud, J.P., Balkanski, Y., Fuzzi, S., Horth, J.,

694   Moortgat, G.K., Winterhalter, R., Myhre, C.E.L., Tsigaridis, K., Vignati, E., Stephanou, E.G., and

695   Wilson, J., 2005: Organic aerosol and global climate modelling: a review. Atmos. Chem. Phys. 5,

696   1053-1123.

697   Kang, H.Q., Zhu, B., Su, J.F., Wang, H.L., Zhang, Q.C., and Wang, F., 2013: Analysis of a long-lasting

698   haze episode in Nanjing, China. Atmos. Res. 120-121, 78-87.

699   Kerminen, V.M., Hillamo, R., Teinila, K., Pakkanen, T., Allegrini, I., Sparapani, R., 2001: Ion balances of

700   size-resolved tropospheric aerosol samples: implications for the acidity and atmospheric processing of

701   aerosols. Atmos. Environ. 35(31), 5255-5265.

702   Koe, L.C.C., Jr, A.F.A., and McGregor, J.L., 2001: Investigating the haze transport from 1997 biomass

703   burning in Southeast Asia: its impact upon Singapore. Atmos. Environ. 35(15), 2723-2734.

704   Lam, S.H.M., Saunders, S.M., Guo, H., Ling, Z.H., Jiang, F., Wang, X.M., and Wang, T.J., 2013:

705   Modelling VOC source impacts on high ozone episode days observed at a mountain summit in Hong

706   Kong under the influence of mountain-valley breezes. Atmos. Environ. 81, 166-176.

707   Lee, E., Chan, C.K., and Paatero, P., 1999: Application of positive matrix factorization in source

708   apportionment of particulate pollutants in Hong Kong. Atmos. Environ. 33, 3201-3212.

709   Lin, Y.C., Cheng, M.T., Lin, W.H., Lan, Y.Y., and Tsuang, B.J., 2010: Causes of the elevated nitrated

710   aerosol levels during episodic days in Taichung urban area, Taiwan. Atmos. Environ. 44, 1632-1640.

711   Ling, Z.H., Guo, H., Lam, S.H.M., Saunders, S.M., Wang, T., 2014: Atmospheric photochemical reactivity

712   and ozone production at two sites in Hong Kong: Application of a Master Chemical

713   Mechanism-photochemical box model. J. Geophys. Res. Atmos. 119, 10567-10582.

714   Liu, Y.J., Zhang, T.T., Liu, Q.Y., Zhang, .R.J., Sun, Z.Q., and Zhang, M.G., 2014: Seasonal variation

715   of physical and chemical properties in TSP, PM_{10} and $PM_{2.5}$ at a roadside site in Beijing and their

716   influence on atmospheric visibility. Aerosol Air Qual. Res. 14, 954-969.

717   Liu, Z.R., Hu, B., Wang, L.L., Wu, F.K., Gao, W.K., and Wang, Y.S., 2015: Seasonal and diurnal

718   variation in particulate matter (PM_{10} and $PM_{2.5}$) at an urban site of Beijing: analyses from a 9-year

719   study. Environ. Sci. Pollut. Res. 22, 627-642.

720   Lyu, X.P., Chen, N., Guo, H., Zhang, W.H., Wang, N., Wang, Y., and Liu, M., 2016: Ambient volatile

721   organic compounds and their effect on ozone production in Wuhan, central China. Sci. Total

722   Environ. 541, 200-209.

723   Lyu, X.P., Ling, Z.H., Guo, H., Saunders, S.M., Lam, S.H.M., Wang, N., Wang, Y., Liu, M., and Wang,

724   T., 2015 (b): Re-examination of C_1–C_5 alkyl nitrates in Hong Kong using an observation-based

725   model. Atmos. Environ. 120, 28-37.

726   Lyu, X.P., Wang, Z.W., Cheng, H.R., Zhang, F., Zhang, G., Wang, X.M., Ling, Z.H., Wang, N., 2015

727   (a): Chemical characteristics of submicron particulates ($PM_{1.0}$) in Wuhan, Central China. Atmos.

728   Res. 161-162, 169-178.

729   Nemesure, S., Wagener, R., and Schwartz, S.E., 1995: Direct shortwave forcing of climate by the

730   anthropogenic sulfate aerosol: sensitivity to particle size, composition, and relative humidity. J.

731   Geophys. Res. 100, 26105-26116.

732   Nriagu, J.O., and Pacyna, J.M., 1988: Quantitative assessment of worldwide contamination of air,

733   water and soils by trace metals. Nature 333, 134-139.

734   Oanh, N.T.K. and Leelasakultum, K., 2011: Analysis of meteorology and emission in haze episode

735   prevalence over mountain-bounded region for early warning. Sci. Total Environ. 409(11),

736   2261-2271.

737   Paatero, P., and Tapper, U., 1994: Positive matrix factorization: A non-negative factor model with optimal

738   utilization of error estimates of data values, Environmetrics 5, 111-126.

739   Paatero, P., 1997: Least squares formulation of robust non-negative factor analysis, Chemom. Intell. Lab.

740   Sys. 37, 23-35.

741   Pathak, R.K., Wang, T., and Wu, W.S., 2011: Nighttime enhancement of $PM_{2.5}$ nitrate in

742   ammonia-poor atmospheric conditions in Beijing and Shanghai: Plausible contributions of

743   heterogeneous hydrolysis of N_2O_5 and HNO_3 partitioning. Atmos. Environ. 45, 1183-1191.

744   Querol, X., Alastuey, A., Viana, M.M., Rodriguez, S., Artinano, B., Salvador, P., Garcia do Santos, S.,

745   Fernandez Patier, R., Ruiz, C.R., de la Rosa, J., Sanchez de la Campa, A., Menendez, M., Gil, J.I.,

746   2004: Speciation and origin of PM_{10} and $PM_{2.5}$ in Spain. J. Aerosol Sci. 35, 1151-1172.

747   Querol, X., Fernandez-Turiel, J.L., and Soler, A.L., 1995: Trace elements in coal and their behavior

748   during combustion in a large power station. Fuel 74, 331-343.

749   Ramanathan, V., Crutzen, P.J., Kiehl, J.T., and Rosenfeld, D., 2001: Aerosol, climate and the

Atmospheric
Chemistry
and Physics
Discussions

Open Access

EGU

750   hydrological cycle. Science 294, 2119-2124.

751   Saarikoski, S., Sillanpaa, M., Sofiev, M., Timonen, H., Saarnio, K., Teinila, K., Karppinen, A.,

752   Kukkonen, J., and Hillamo, R., 2007: Chemical composition of aerosols during a major biomass

753   burning episode over northern Europe in spring 2006: Experimental and modelling assessments.

754   Atmos. Environ. 41, 3577-3589.

755   Seinfeld, J.H., and Pandis, S.N., 1998: Atmospheric chemistry and physics from air pollution to

756   climate change. Wiley, New York, p. 528.

757   Shen, G.F., Yuan, S.Y., Xie, Y.N., Xia, S.J., Li, L., Yao, Y.K., Qiao, Y.Z., Zhang, J., Zhao, .Q.Y., Ding, A.J.,

758   Li, B., and Wu, H.S., 2014: Ambient levels and temporal variations of PM2.5 and PM10 at a residential

759   site in the mega-city, Nanjing, in the western Yangtze River Delta, China. J. Environ. Sci. Health: Part A

760   49(2), 171-178.

761   Shen, Z.X., Cao, J.J., Liu, S.X., Zhu, C.S., Wang, X., Zhang, T., Xu, H.M., Hu, T.F., 2011: Chemical

762   compositions of PM_{10} and $PM_{2.5}$ collected at ground level and 100 meters during a strong winter-time

763   pollution episode in Xi'an, China. J Air Waste Manage. Assoc. 61(11), 1150-1159.

764   Simoneit, B.R.T., 2002: Biomass burning-a review of organic tracers for smoke from incomplete

765   combustion. Appl. Geochem. 17(3), 129-162.

766   Tang, I.N., Munkelwitz, H.R., 1993: Compositions and temperature dependence of the deliquescence

767   properties of hygroscopic aerosols. Atmos. Environ. 27, 467-473.

768   Theodosi, C., Grivas, G., Zarmpas, P., Chaloulakou, A., and Mihalopoulos, N., 2011: Mass and

769   chemical composition of size-segregated aerosols (PM_1, $PM_{2.5}$, PM_{10}) over Athens, Greece: local

770   versus regional sources. Atmos. Chem. Phys. 11, 11895-1191.

771   Wang, H., Tan, S.C., Wang, Y., Jiang, C., Shi, G.Y., Zhang, M.X., and Che, H.Z., 2014 (a): A

772   multisource observation study of the severe prolonged regional haze episode over eastern China in

773   January 2013. Atmos. Environ. 89, 807-815.

774   Wang, H., Xu, J.Y., Zhang, M., Yang, Y.Q., Shen, X.J., Wang, Y.Q., Chen, D., and Guo, J.P., 2014 (b):

775   A study of the meteorological causes of a prolonged and severe haze episode in January 2013 over

776   central-eastern China. Atmos. Environ. 98, 146-157.

777   Wang, H.L., Lou, S.R., Huang, C., Qiao, L.P., Tang, X.B., Chen, C.H., Zeng, L.M., Wang, Q., Zhou,

778   M., Lu, S.H., and Yu, X.N., 2014: Source profiles of volatile organic compounds from biomass

779   burning in Yangtze River Delta, China. Aerosol Air Qual. Res. 14, 818-828.

Atmospheric
Chemistry
and Physics
Discussions

780   Wang, J., Hu, Z.M., Chen, Y.Y., Chen, Z.L., and Xu, S.Y., 2013: Contamination characteristics and

781   possible sources of PM_{10} and $PM_{2.5}$ in different functional areas of Shanghai, China. Atmos.

782   Environ. 68, 221-229.

783   Wang, P., Cao, J.J., Tie, X.X., Wang, G.H., Li, G.H., Hu, T.F., Wu, Y.T., Xu, Y.S., Xu, G.D., Zhao,

784   Y.Z., Ding, W.C., Liu, H.K., Huang, R.J., and Zhan, C.L., 2015: Impact of meteorological

785   parameters and gaseous pollutants on PM2.5 and PM10 mass concentrations during 2010 in Xi'an,

786   China. Aerosol Air Qual. Res. 15, 1844-1854.

787   Wang, Y.X., Zhang, Q.Q., Jiang, J.K., Zhou, W., Wang, B.Y., He, K.B., Duan, F.K., Zhang, Q., Philip,

788   S., Xie, Y.Y., 2014: Enhanced sulfate formation during China's severe winter haze episode in

789   January 2013 missing from current models. J. Geophys. Res. 119, 10425-10440.

790   White W.H. and Roberts, P.T., 1977: On the nature and origins of visibility-reducing aerosols in the

791   los angeles air basin. Atmos. Environ. 11(9), 803-812.

792   Wuhan Environmental Bulletin, 2014, accessible at http://www.whepb.gov.cn/zwGkhjtj/ 16240.jhtml.

793   Yang, L.X., Zhou, X.H., Wang, Z., Zhou, Y., Cheng, S.H., Xu, P.J., Gao, X.M., Nie, W., Wang, X.F.,

794   and Wang, W.X., 2012: Airborne fine particulate pollution in Jinan, China: Concentrations,

795   chemical compositions and influence on visibility impairment. Atmos. Environ. 55, 506-514.

796   Yao, X.H., Chan, C.K., Fang, M., Candle, S., Chan, T., Mulawa, P., He, K.B., and Ye, B., 2002: The

797   water-soluble ionic composition of $PM_{2.5}$ in Shanghai and Beijing, China. Atmos. Environ. 36(26),

798   4223-4234.

799   Zhang, F., Cheng, H.R., Wang, Z.W., Lv, X.P., Zhu, Z.M., Zhang, G., and Wang, X.M., 2014: Fine

800   particles ($PM_{2.5}$) at a CAWNET background site in Central China: Chemical compositions, seasonal

801   variations and regional pollution events. Atmos. Environ. 86, 193-202.

802   Zhang, G.H., Bi, X.H., Chan, L.Y., Wang, X.M., Sheng, G.Y., and Fu, J.M., 2013: Size-segregated

803   chemical characteristics of aerosol during haze in an urban area of the Pearl River Delta region,

804   China. Urban Climate 4, 74-84.

805   Zhang, Q., Jimenez, J.L., Worsnop, D.R., Canagaratna, M., 2007: A case study of urban particle

806   acidity and its influence on secondary organic aerosol. Environ. Sci. Technol. 41(9), 3213-3219.

807   Zhang, X.Y., Wang, Y.Q., Niu, T., Zhang, X.C., Gong, S.L., Zhang, Y.M., and Sun, J.Y., 2012:

808   Atmospheric aerosol compositions in China: spatial/temporal variability, chemical signature,

809   regional haze distribution and comparisons with global aerosols. Atmos. Chem. Phys. 12, 779-799.

810   Zhang, Y.Y., Obrist, D., Zielinska, B., and Gertler, A., 2013: Particulate emissions from different types

811   of biomass burning. Atmos. Environ. 72, 27-35.

812   Zheng, M., Salmon, L.G., Schauer, J.J., Zeng, L.M., Kiang, C.S., Zhang, Y.H., Cass, G.R., 2005:

813   Seasonal trends in $PM_{2.5}$ source contributions in Beijing, China. Atmos. Environ. 39(22),

814   3967-3976.